energies

MDPI

Article

Numerical-Well-Testing Interpretation of Injection/Falloff Testing for Coalbed Methane Well in Hedong Coalfield

Shiyue Fang [1], Xujing Zhang [1,*], Xinzhan Li [2], Yue Chen [1], Baiyi He [3], Yuan Bao [1] and Dongmin Ma [1]

[1] College of Geology and Environment, Xi'an University of Science & Technology, Xi'an 710054, China; fangshiyue@xust.edu.cn (S.F.); cyxust@126.com (Y.C.); y.bao@foxmail.com (Y.B.); mdm6757@126.com (D.M.)
[2] National Pipe Network Group United Pipeline Co., Ltd., West East Gas Transmiss Gansu-Shaanxi Branch, Xi'an 710021, China; xsylxz@163.com
[3] National Pipe Network Group United Pipeline Co., Ltd., West East Gas Transmiss Yinchuang Branch, Yinchuang 750001, China; heby01@pipechina.com.cn
* Correspondence: zhangxujing0715@163.com; Tel.: +86-13466801499

Abstract: Numerical well testing is used mostly in oil/gas, geothermal, and coalbed methane injection/falloff well-testing interpretations while few published studies have been presented on how to adjust the models and numerical experiments parameters. Meanwhile, there is no simple and highly applicable evaluation standard on the approximation degree between the simulated and field-measured pressure response. In this paper, seven groups of numerical experiments were conducted to obtain the simulated pressure response. The Pearson correlation coefficients and the grey correlation between the simulated and field-measured pressure response were calculated to evaluate the approximation degree. In homogeneous, stress-independent, multi-layered, heterogeneous and integrated models, the simulated pressure response curves all fit to the field data well at the early and late time of the falloff period. However, the highest approximation degree was only found in the integrated model. Finally, the permeability, initial pressure, skin factor and investigation radius of the tested CBM reservoir were determined. The results show that, to obtain a reliable interpretation result, it is best to give an approximation degree evaluation standard on the approximation degree between the simulated and field-measured pressure response, build an integrated numerical model, and input the correct parameters, such as the effective thickness and the testing fluid viscosity. Otherwise, it will also drop into a pitfall of multi-results. The method we used is very relevant to CBM exploration and safe mining in Hedong coalfield.

Keywords: IFOT; log–log diagnostic; numerical well testing; CBM well; approximation degree

Citation: Fang, S.; Zhang, X.; Li, X.; Chen, Y.; He, B.; Bao, Y.; Ma, D. Numerical-Well-Testing Interpretation of Injection/Falloff Testing for Coalbed Methane Well in Hedong Coalfield. *Energies* **2023**, *16*, 4864. https://doi.org/10.3390/en16134864

Academic Editors: Shu Tao, Huazhou Huang, Shuoliang Wang and Yanjun Meng

Received: 1 June 2023
Revised: 18 June 2023
Accepted: 18 June 2023
Published: 22 June 2023

1. Introduction

Since injection/falloff testing (IFOT) was used firstly in 1989 [1], it has been widely and successfully applied to obtain reservoir parameters such as permeability, skin factor and initial pressure [2]. During the interpretation of IFOT, the Horner curve and the log–log diagnostic analysis are the frequently used methods. However, they are based on semi-analytical models with many set restrictions for simplifying [3,4]. Therefore, numerical-well-testing interpretation has been put forward recently. It can be based on a true reservoir model. Complex boundaries, heterogeneity, and multi-layered and complex flow mechanisms can be conveniently considered [4,5]. Given this, numerical-well-testing interpretation is used mostly in oil/gas and geothermal IFOT well testing [4–7]. Numerical well testing has also been used in coalbed methane (CBM) IFOT in the past two decades [7–10]; however, few studies have focused on the adjustment process during numerical experiments and interpretation.

During numerical well testing, parameters, computational models and numerical methods are often adjusted to find a nearest simulated pressure response curve to the field-measured data. However, how to find this nearest curve or give a standard to evaluate

the approximation degree between the simulated data and field data is the first and most important consideration. Unfortunately, few applicable evaluation criteria exist due to the low accuracy and applicability of CBM IFOT numerical-well-testing interpretation, although the history match method [11] is the most used. At same time, few descriptions on the better computational model and the appropriate parameters input into the numerical model, such as the effective thickness and viscosity of the testing fluid, have been observed, which are crucial to the well testing interpretation.

In this study, the IFOT method was firstly used to obtain the field data of the pressure response in the CBM of Hedong coalfield. Then, seven groups of numerical experiments were conducted on a finite element simulation tool named Parallel Adaptive Nonlinear Deformation Analysis Software (PANDAS), which can run on a normal computer, although a supercomputer was often used to simulate dynamic processes in reservoirs [4,7,12–14].The simulated pressure response were obtained in a homogeneous, stress-dependent, multi-layered, heterogeneous and integrated model. The Pearson correlation coefficients (r_p, confidence degree $\alpha = 0.01$) and gray correlation degree (γ_{0i}) were calculated, respectively, to measure the approximation degree between the simulated pressure response and field-measured data [15]. At same time, the Horner curve and log–log analysis were used to obtain the reservoir parameters in every model. Finally, the most reasonable simulated pressure response was selected to obtain the most reliable interpretation results of the well V01.

The method we employed will not only help us understand the testing fluid flow in CBM reservoirs but also be able to improve the interpretation accuracy during IFOT. It will be very conducive to the exploration and extraction of CBM [16]. It will also help to reduce the danger of methane explosion or aerologic risks and obtain greater reliability for safe mining [14].

2. Methodology

2.1. Field Data Acquisition

The V01 well is located in Shilou North block, Hedong coalfield, eastern margin of the Ordos Basin, China. The main coal-bearing sequences of V01 well are Taiyuan Formation and Shanxi Formation which strike northwest and dip to the southeast at an angle of 2°–5°. Coal seam No. 9+10 is the tested formation. According to drilling data, its burial depth is from 787.56 m to 790.96 m and the reservoir thickness is 2.50 m. It has two inter-layer and three coal delaminations [17]. The thicknesses are 0.60 m, 0.30 m, 0.75 m, 1.13 m and 0.62 m, respectively, which are shown in Figure 1.

Across China, hundreds of CBM wells have been used in more than 30 CBM Basins by using the IFOT method [18]. The V01 well, which is a 0.06 m radius barefoot well, was also tested by this test technique. The whole testing process was carried out after the Chinese National Standard GB 24504–2009/T [19], which included two main steps as follows [20].

Step 1: Water was injected into the well with an average rate of 0.087 m^3/d. The injection continued 13.25 h and the cumulative volume of injected water was 0.048 m^3.

Step 2: The well was closed by the shut-in valve in the bottom hole to obtain the falloff pressure. This process lasted 26.17 h. The field pressure response data are shown in Figure 2.

The software Origin lab 9.0 was employed to analyze the falloff pressure-time data by Horner curve and Log–log diagnosis analysis, which is shown in Figure 2a,b. From the level part of the pressure derivate ($\Delta p' \cdot t$) curve in Figure 2b, we can find a corresponding straight line on the Horner curve by using the value of $\log\left[\frac{t_p+\Delta t}{\Delta t}\right]$, namely, the green line. However, its slope is equal to 2.0. Another straight line should be found on the Horner curve, namely, the red line; after all, it must agree to the relation $t_p + \Delta t \cong \Delta t$. However, it is not in line with the log–log curve. From the linear fitting course, we can see that the conventional testing interpretation can easily drop into the pitfall described in the literature [2]. It indicates that another testing interpretation method should be found to obtain the reliable reservoir parameters, at least, in the V01 well. Hence, the numerical-

well-testing interpretation was employed in this study. However, it is worth pointing out that the conventional testing interpretation can obtain the reservoir parameter roughly. It is conducive to the numerical well testing. Using the formulae given in the literature [3,7], the slope of the Horner curve, the permeability, the radius of investigation can be calculated roughly, which are 0.0734 md and 7.3689 m, respectively. The initial pressure of coal seam No. 9+10 can be read from the intercept of straight line which slope is equal to 1.0.

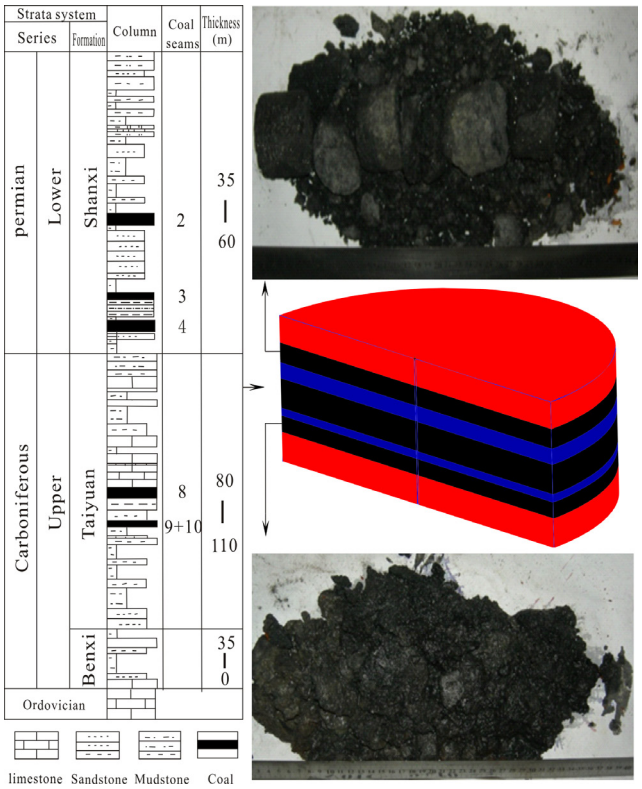

Figure 1. Coal-bearing sequences in the tested well and structure of coal seam No. 9+10.

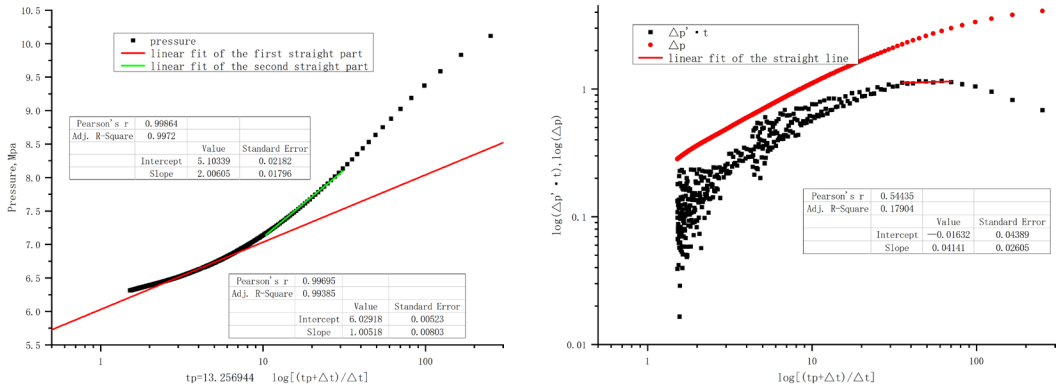

(**a**) Horner curve (**b**) Log–log diagnostic plot

Figure 2. Log–log diagnostic analysis plots of the tested well.

2.2. Numerical-Well-Testing Interpretation

To obtain more reliable reservoir parameters and investigate the testing fluid flow in CBM reservoir during IFOT, seven groups of numerical simulation were conducted on PANDAS.

2.2.1. Governing Equations

If the theory is based on a cylindrical reservoir with a vertical well at the center and the thermal effects is omitted, the testing fluid flow in the CBM reservoir during IFOT can be expressed by the following equations [4,7,9–11,18,20–22]:

$$\frac{\partial^2 p}{\partial r^2} + \frac{1}{r}\frac{\partial p}{\partial r} + q = \frac{\phi C_t \mu}{K}\frac{\partial p}{\partial t} \tag{1}$$

where p is the fluid pressure, MPa; q is flow rate on the ground, m^3/s; r is radial distance, m; ϕ is porosity; C_t is total compressibility, Mpa^{-1}; μ is viscosity, mpa.s; K is permeability, md; t is time, s.

The initial conditions

$$p\Big|_{(t=0)} = p_i \tag{2}$$

where p_i is the initial pressure, MPa.

The infinite boundary

$$p|(r \to \infty) = 0 \tag{3}$$

The constant pressure outer boundary

$$p|(r \to r_e) = p_e \tag{4}$$

where r_e is the external radius, m; p_e is external boundary pressure, MPa.

The inner boundary

$$q = \frac{h}{\mu}\int_0^{2\pi} k(r_w,\theta)\frac{\partial p(r_w,\theta)}{\partial r} r_w d\theta \tag{5}$$

where h is effective thickness, m; r_w is wellbore radius, m; θ is angle, rad.

2.2.2. Models and Main Parameters

According to the structure of the tested coal seam in the V01 well, a plate-like multi-layered porous medium model was built. By comparison and simplification, a plate-like single-layer was also built, which is most used in the Horner curve and Log–log diagnosis analysis. In all models, the inner radius of numerical models was set as 60 mm (see Figure 3a) according to the V01 well structure. Considering that the investigation radius is generally less than 10 m during IFOT [1–3,18,20], the outer radius was built as 10,000 mm in the computational models.

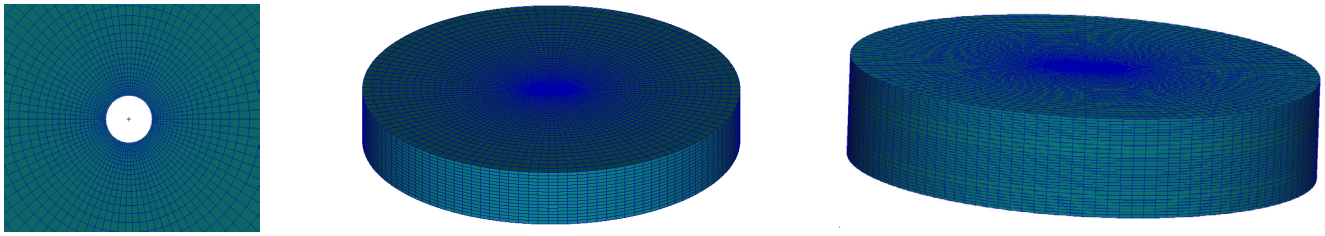

(**a**) Well in the center (**b**) Single-layer model (**c**) Multilayer model

Figure 3. Simulation model of injection/falloff testing.

The surface elements were extruded and swept to the different-thickness porous medium models with HEX8 (eight-node hexahedron) solid elements, which are shown in Figure 3b and Table 1. A 3400 mm thick multi-layered model was made with five layers (see Figure 3c). From the bottom to top, the thicknesses were 620 mm, 300 mm, 1130 mm, 600 mm and 750 mm, successively. Among them, the 300 mm thick and 600 mm thick plates were the inter-layers, and the others were coal delaminations No. 1 to No. 3. The outer and

inner radii were the same as the single-layer model. The whole model was discretized into 192,000 HEX8 solid elements and the node number reached up to 2,238,327.

Table 1. Main parameters in the numerical simulation.

Grid Properties of Model				Properties of Testing Fluid		Properties of Tested Coalbed	
Module Number	**Thickness (mm)**	**Element Number**	**Node Number**	**Parameter Name**	**Value**	**Parameter Name**	**Value**
No. 1	2500	96,000	104,040	Viscosity (mpa·s)	1	Porosity	3%
No. 2	1130	48,000	55,080	Compressibility (Mpa^{-1})	4.35×10^{-4}	Compressibility (Mpa^{-1})	0.65×10^{-4}
No. 3	750	30,000	36,720	Injection rate (m^3/d)	0.087	Well volume (m^3)	9.04
No. 4	620	24,000	30,600	Density (kg/m^3)	1000	Shut-in well volume (m^3)	0.719

Most parameters in the numerical simulation came from field testing. The earlier research in Hedong coalfield [17] or the adjacent block of the Ordos Basin [15,18,20,21] were also referred to. Considering the above analysis in Section 2.1, the main parameters in the single-layer model are listed in Table 1. Considering the earlier research [16–18,20–22] and the relationship between the burial depth and porous-flow-mechanic parameters, the main parameters of the coalbed in the multilayer and stress-independent model are shown in Table 2. The properties of interlayers are three orders of magnitude less than those in the coalbed. It should be noted that the parameters input into the numerical models determined by experiments or logging were the best possible, although we read them from the reference in part.

Table 2. Main parameters of coalbed in multilayer and stress-independent model.

Coal Delamination No. 1		Coal Delamination No. 2		Coal Delamination No. 3	
Permeability (md)	0.045	Permeability (md)	0.0425	Permeability (md)	0.040
Porosity (%)	3	Porosity (%)	3	Porosity (%)	3
Compressibility (Mpa^{-1})	0.70×10^{-4}	Compressibility (Mpa^{-1})	0.65×10^{-4}	Compressibility (Mpa^{-1})	0.60×10^{-4}
Young's module (Gpa)	1.25	Young's module	1.33	Young's module	1.52
Passion ratio	0.35	Passion ratio	0.33	Passion ratio	0.31

The stress dependence of coal permeability is a commonly observed and generally accepted dynamic behavior [8,10,22–26]. According to John Seidle [3], the Palmer–Mansoori porosity relation [25] can be written as

$$\frac{\phi}{\phi_0} = 1 + \frac{(1+v)(1-2v)}{(1-v)E\phi_0}(p-p_0) + \frac{c_0}{\phi_0} * \frac{2(1-2v)}{3(1-v)}\left(\frac{p_0}{p_0+p_L} - \frac{p}{p+p_L}\right) \quad (6)$$

where ϕ_0 is porosity at virgin reservoir pressure, fraction; v is the Poisson's ratio; E is Young's module; p_0 is the original reservoir pressure, MPa; c_0 is the volumetric strain coefficient, Mpa^{-1}; p_L is the Langmuir pressure, MPa.

The permeability varies with porosity as follow [10,25].

$$\frac{k}{k_0} = \left(\frac{\phi}{\phi_0}\right)^3 \quad (7)$$

where k_0 is the permeability at virgin reservoir pressure.

If grain compressibility is very small, and the matrix shrinkage can be neglected, Equation (6) becomes

$$\frac{\phi}{\phi_0} = 1 + \frac{(1+v)(1-2v)}{(1-v)E\phi_0}(p-p_0) \quad (8)$$

Palmer and Mansoori [25] also gave the other equations, which were derived from the fundamental reservoir parameters to predict how permeability changes with stress or

pore pressure during falloff or injection. If the matrix shrinkage can be neglected, the pore volume compressibility C_{fu} is constant [3,7,10,22–26].

$$C_{fu} = \frac{(1+v)(1-2v)}{(1-v)E\phi_0} \tag{9}$$

$$\frac{k}{k_0} = exp\left[3C_{fu}(P-P_0)\right] \tag{10}$$

In a stress-dependent model and integrated model, these equations were used to investigate the stress-sensitive effect in the CBM reservoir. These equations were divided into three groups: (6) and (7), (7) and (8), and (9) and (10). Therefore, three groups of numerical experiments were performed because of the different calculation on permeability and porosity in the stress-dependent model.

2.2.3. Approximation Degree Measuring

To measure the approximation degree between the simulated pressure response and field-measured data, Pearson correlation coefficients (r_p, confidence degree α = 0.01) and the gray correlation were calculated, respectively. The former can estimate the correlation and the latter can measure the consistency of the variation trend between the simulated data and field data. According to the statistical and gray-system theory, the bigger the r_p value, the higher the correlation between simulated data and field data is. Similarly, the bigger the gray correlation is, the higher the synchronization degree is [15,27,28]. Because the sampling interval of the field data is 5 s at the early time and 20 s at the late time of the falloff period, while the sampling intervals of the simulated pressure response are different to each other and also different to the field data, the gray correlation degree is difficult to obtain. Therefore, the field data were compressed at every 200 s at early time and 800 s at late time. The simulated data are interpolated at the same sampling interval to the field compressed data. The interpolation method we used was the cubic B-spline.

The calculation of Pearson correlation coefficients can be carried out in Origin lab 9.0. The grey correlation analysis was carried out on a VB applet written by some professors in our college. The calculation steps are shown as follows [14,26,27]:

Step 1: Establish the original matrix x_i of field-measured and simulated pressure response by Formula (11):

$$x_i = (x_i(0), x_i(1), \ldots, x_i(k)) \tag{11}$$

where $x_i(0)$ is the field-measured data, $x_i(k)$ is the simulated pressure response.

Step 2: Calculate the Pearson correlation coefficients by using the Formula (12).

$$r_p = \sum_{i=1}^{n}\left(x_i(0) - \overline{x_i(0)}\right)\left(x_k(0) - \overline{x_k(0)}\right) / \left(\sqrt{\sum_{i=1}^{n}\left(x_i(0) - \overline{x_i(0)}\right)^2} \cdot \sqrt{\sum_{i=1}^{n}\left(x_k(0) - \overline{x_k(0)}\right)^2}\right) \tag{12}$$

where n is the total number of the sample, and $\overline{x_i(0)}$ and $\overline{x_k(0)}$ are the mean of the sample.

Step 3: Evaluate the initialization transformed matrix x_i' by using Formula (13):

$$x_i' = \left(\frac{x_i(0)}{x_i(0)}, \frac{x_i(1)}{x_i(0)}, \frac{x_i(2)}{x_i(0)}, \ldots, \frac{x_i(k)}{x_i(0)}\right) \tag{13}$$

Step 4: Evaluate the difference sequence $\Delta_{0i}(k)$ using Formula (14):

$$\Delta_{0i}(k) = \left|x_0'(0) - x_i'(k)\right| \tag{14}$$

Step 5: Calculate the correlation coefficient $\xi_{0i}(k)$ and the grey correlation degree γ_{0i} using Formulaes (15) and (16):

$$\xi_{0i}(k) = \frac{min_i min_k \Delta_{0i}(k) + \varphi max_i max_k \Delta_{0i}(k)}{\Delta_{0i}(k) + \varphi max_i max_k \Delta_{0i}(k)} \quad (15)$$

$$\gamma_{0i} = \frac{1}{n-1} \sum_{k=1}^{n} \xi_{0i}(k) \quad (16)$$

where the resolution ratio ($\varphi = 0.5$) is used to improve the significance of the difference between the correlation coefficients.

2.2.4. Calculation of Reservoir Parameters

In every model, permeability can be exported when the simulated pressure–time curve with high Pearson correlation coefficients and a high grey correlation is obtained. In view of the well shut in the bottom, the well-bore storage factor is near to zero. Therefore, the well-bore storage factor is not investigated. Investigation radius can be read from the pressure distribution plots. Using the simulated pressure response, the initial pressure and skin factor can be calculated by the Horner curve and log–log analysis, which the detail steps have shown in the Section 2.1.

3. Results

3.1. Homogeneous Model

The simulated results of the tested well are shown in Figure 4, in the case in which the reservoir was 2500 mm thick and homogeneous.

From Figure 4a, it can be seen that the simulated data match with the field data well at the early time of the fall-off period, except the maximum pressure. Although there is inconformity at mid- and late-falloff, most data are close to the field data. The Pearson correlation coefficient is 0.9784 and the gray correlation is 0.448.

Figure 4b shows that the pressure decreases with an increasing radius value. The high pressure is located near to the wellbore. The velocity increases with the radius value. The high velocity is near the boundary but not at the boundary. Meanwhile, the investigation radius can be read from Figure 4b, which is 9.495 m. From the Horner curve shown in Figure 4c, the initial pressure is 6.0097 Mpa and 0.0403 Mpa. The permeability is 0.0667 md which has a gap of 0.0067 md to that we obtained from the field data. The skin factor is 6.614 Mpa. The pressure change and derivative curves corresponding to the fall-off period are plotted in Figure 4d. From Figure 4d, long obvious radial flow characteristics are identified. Meanwhile, the type of curve can be divided into three parts based on its characteristics in different stages [3,7]. The first part is the wellbore control section line with the slope 0.82217. The second part is an approximate horizontal line of slope 0.13902 with a radial fluid flow around the wellbore. The third part is the straight line with the negative slope −0.57551, showing the effect of the constant pressure outer boundary.

3.2. Effect of Stress Sensitivity

The simulated results of the tested well are shown in Figure 5, if the reservoir is 2500 mm thick, homogeneous and the effect of stress sensitivity is taken into consideration.

As can be seen from Figure 5a, a small difference exists among these three experiments at early and late time of the fall-off period. Pressure–time curves almost overlap each other. However, a discrepancy can be seen at the middle time of the falloff period when the zoom graph is given. Their Pearson correlation coefficients are 0.96705 (matrix shrinkage is neglected), 0.97596 (strong matrix shrinkage is taken into consideration) and 0.97076 (constant pore compressibility is assumed), respectively. The gray correlation degrees are 0.375, 0.412 and 0.405, respectively. It indicates that the tested coal seam is stress-dependent and strong matrix shrinkage should be taken into consideration. Hence, the simulated pressure response (strong matrix shrinkage is taken into consideration) was

applied to conduct the log–log analysis. The results are shown in Figure 5b. This curve can be divided into four parts. The first part is the wellbore control section line with the slope 0.7247 which is near to 1. The second part is a complicated "hump-shape" curve with a stress-independent effect. The third part is an approximate horizontal line of slope 0.037 (near to zero) with a radial fluid flow around the wellbore. The fourth part is the straight line with the negative slope (−0.3362), showing the effect of the constant-pressure outer boundary.

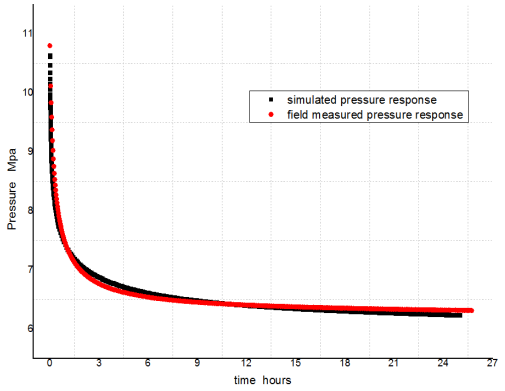

(**a**) pressure–time curves

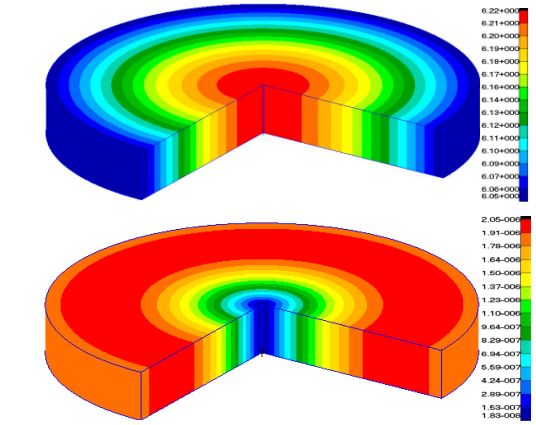

(**b**) pressure/velocity distribution at the end of falloff period

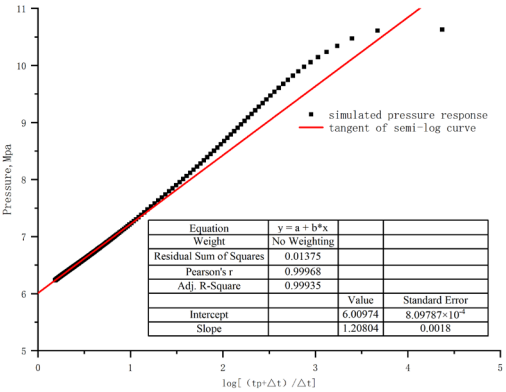

(**c**) Semi-log plot

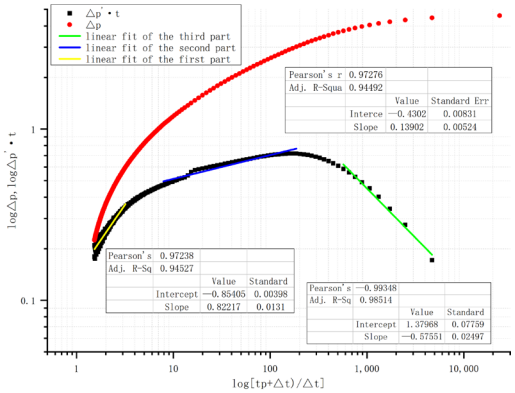

(**d**) Log–log plot

Figure 4. Simulated results in homogeneous model.

The Horner curves are shown in Figure 5c. At the early time, the curves overlap each other, while they separate at the mid- and late-time. If the pressure response of the early time is used to obtain the reservoir parameters, it will drop into a trough and we would obtain incorrect results. Referring to the log–log diagnosis plot, the permeability is 0.0756 md, which is 0.0022 md larger than that which we obtained from the field-measured pressure response. The initial pressure is 6.002 Mpa and the skin factor is 7.583. The pressure distributions in these three experiments were almost same, and are shown in Figure 5d. From that, we can see that the investigated radius is 9.495 m.

From Figure 5e–g, it can be seen that the velocity distribution patterns are also same but the values are different. Among them, the v_{max} is the biggest if strong matrix shrinkage is taken into consideration. However, it is smallest if the matrix shrinkage is neglected. The v_{min} is smallest in the strong-matrix-shrinkage model and the biggest in the model of constant pore volume compressibility. These demonstrate that the flow resistance gradient increases when the matrix shrinkage is taken into consideration. However, it is not big enough to affect the pressure distribution. It may draw our attention to improve the measurement accuracy of the pressure gauge or change the measured specification to detect the stress-independent effect during IFOT in the CBM well.

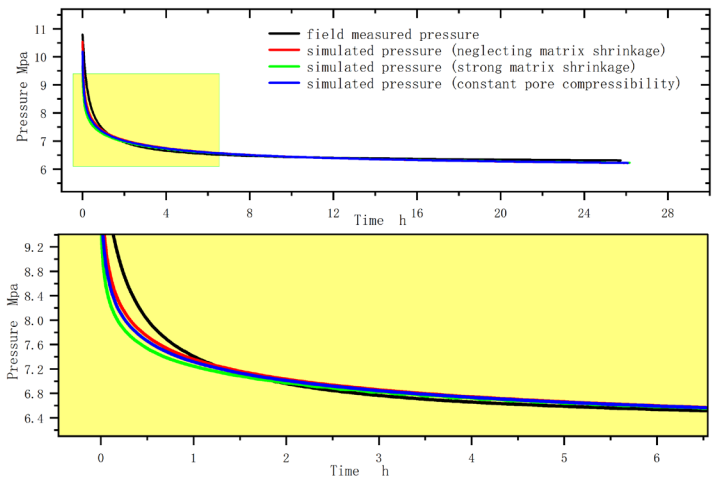

(**a**) Pressure–time curves

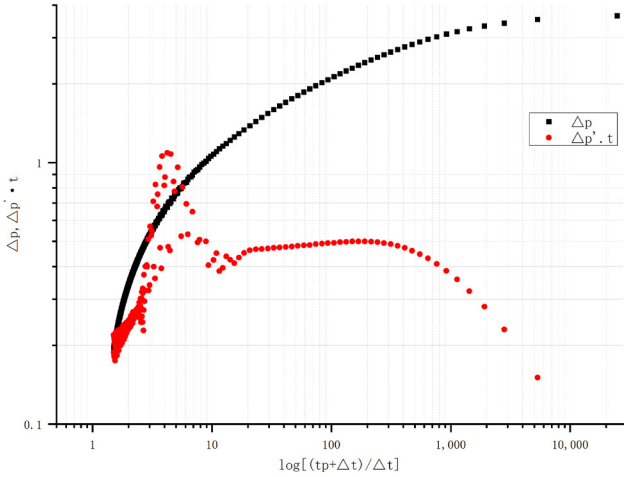

(**b**) Log–log plot

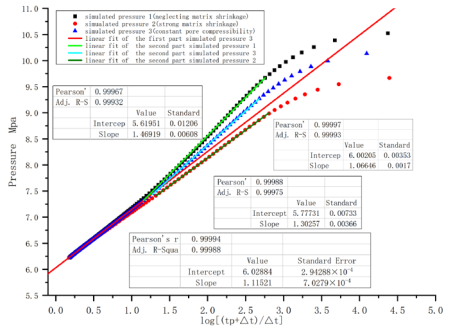

(**c**) Horner curves

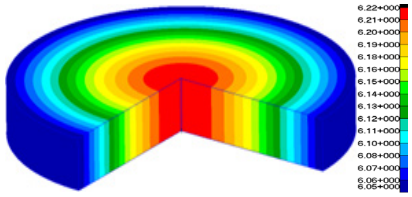

(**d**) Pressure distribution at end of falloff

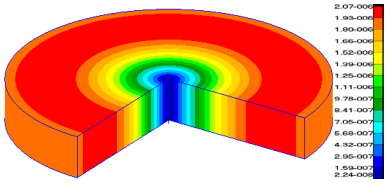

(**e**) Velocity distribution with constant Cp

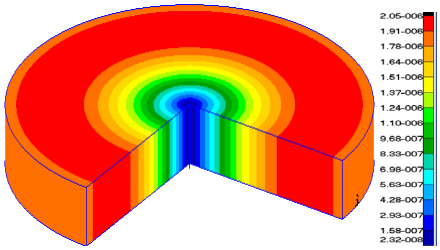

(**f**) Velocity distribution (neglecting matrix shrinkage)

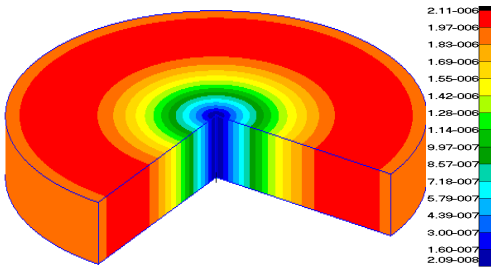

(**g**) Velocity distribution (strong matrix shrinkage)

Figure 5. Simulated results in stress-independent model.

3.3. Multi-Layered Model

From Figure 6a, it can be concluded that, at the early and middle falloff, the simulated pressure response fits the field data well. However, at late falloff, the simulated data do not match with it, although the Pearson correlation coefficient is 0.96717 and the gray correlation degree is 0.604. This may imply that there might be some other factors which were not considered. Figure 6b shows that the pressure and velocity distribution are similar in every formation. At the end of falloff, the pressure and velocity contour are slightly different in every formation. The same pressure and velocity are located differently which are proportional to the permeability and inverse to the compressibility. It may imply that

"fingering flow" will come out if the property difference among formations becomes bigger. From the pressure distribution at the end of falloff period, the investigated radius can be read, which is 9.002 m.

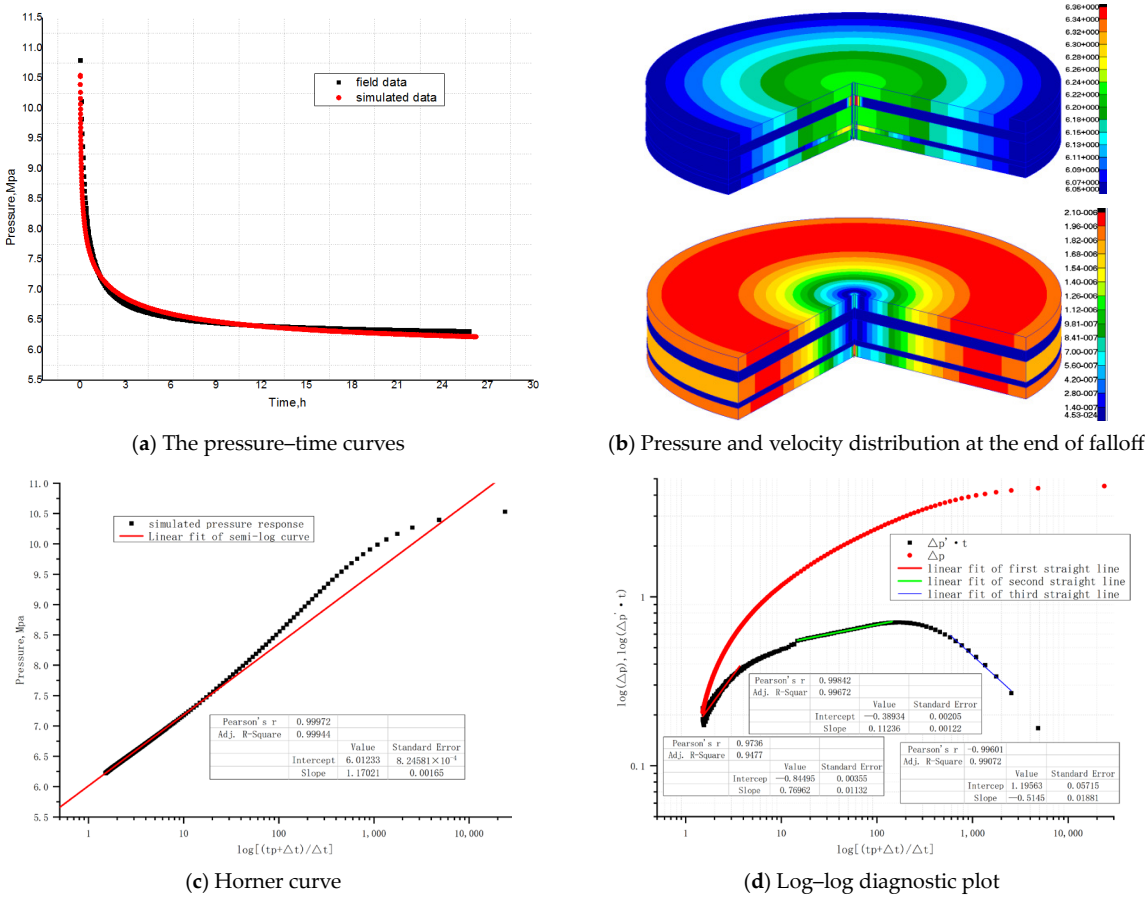

(**a**) The pressure–time curves

(**b**) Pressure and velocity distribution at the end of falloff

(**c**) Horner curve

(**d**) Log–log diagnostic plot

Figure 6. The simulated results in multi-layered model.

The equivalent permeability can be calculated as 0.0689 md which is 0.0045 md smaller than that we obtained from the field data. It can also be calculated by the weighted average method according to the layer thickness, which has value of 0.04357 md. The initial pressure is 6.01233 Mpa and the skin factor is 8.021. In the log–log diagnostic plot (Figure 6d), the curve can also be divided into three parts which the same as in the 2500 mm thick homogenous model. However, the slopes are different. These are 0.76962, 0.11236 and −0.51456, respectively.

3.4. Heterogeneous Model

The simulated results in the heterogeneous model are shown in Figure 7. As can be seen from Figure 7a, the simulated pressure response curve deviates from the field data at the middle falloff when the permeability in the x direction is not equal to that in the y direction. With the increasing value of the $\frac{k_x}{k_y}$ ratio, the simulated data departs further from the field data. The Pearson correlation coefficients are 0.96425, 0.95863 and 0.96542 when the values of $\frac{k_x}{k_y}$ ratio are 1.1, 3.0 and 10, respectively. This indicates that the high value of Pearson correlation coefficients does not guarantee the high proximity between the simulated pressure response and field-measured data. That is why the grey correlation degree is employed to evaluate the proximity. Their grey correlation degree to the field data are 0.715, 0.621 and 0.411 in these three numerical experiments. From the value of grey correlation degree, the tested coal seam in well V01 can be thought of as weakly heterogeneous.

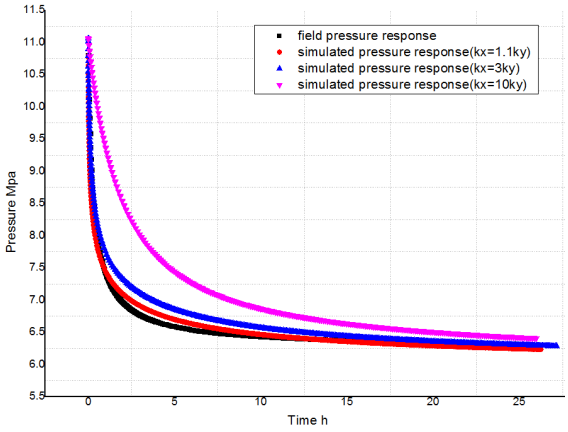

(**a**) Pressure–time curves of different permeability ratios

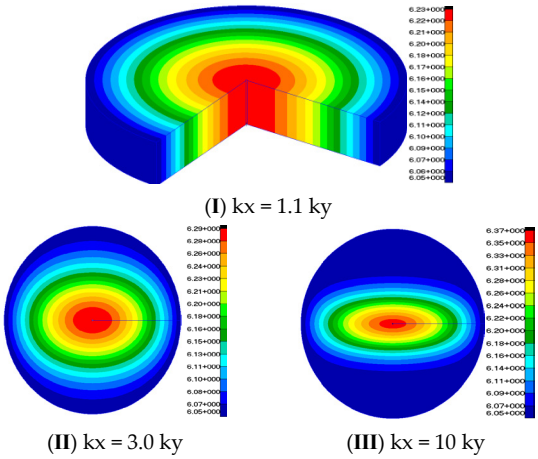

(**I**) kx = 1.1 ky

(**II**) kx = 3.0 ky (**III**) kx = 10 ky

(**b**) Pressure distribution at the end of the falloff period

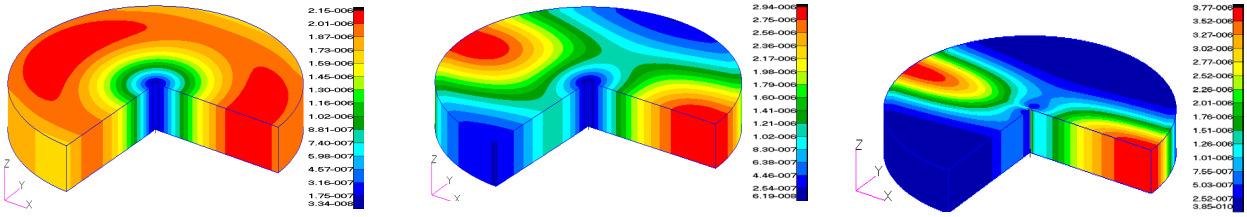

(**I**) kx = 1.1 ky (**II**) kx = 3.0 ky (**III**) kx = 10 ky

(**c**) Velocity distribution at the end of the falloff period

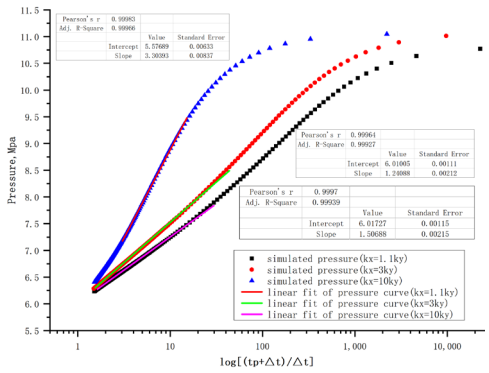

(**d**) Horner curves

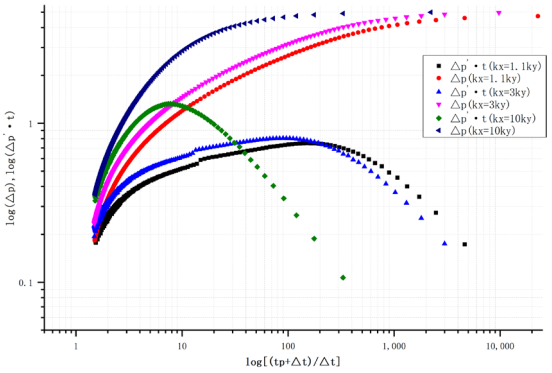

(**e**) Log–log diagnostic plots

Figure 7. Simulated results in the heterogeneous model.

From Figure 7b, it can be seen that the pressure near the wellbore becomes slightly bigger with the increasing value of the $\frac{k_x}{k_y}$ ratio at the end of the falloff period, with values of 6.23 Mpa, 6.29 Mpa and 6.37 Mpa, respectively. The investigation radii in these three numerical experiments have almost same value which is 9.497 m. The flow forms an "egg shape" near the wellbore, and forms an ellipse shape at the area distant from the well. The major axis radius of the ellipse increases with the increasing value of the $\frac{k_x}{k_y}$ ratio. It can be considered that the propagation speed of the pressure in the x direction is faster than that in any other direction owing to its much bigger permeability. Figure 7c shows that the v_{max} also becomes bigger with the increasing value of the $\frac{k_x}{k_y}$ ratio. From the pressure–time curves and pressure/velocity distribution in the heterogeneous model, the conclusion can be drawn at that the CBM reservoir in well V01 is a weak heterogeneous coal seam.

According to Figure 7d, the permeability values of these three numerical experiments are 0.065 md, 0.0535 md and 0.0244 md, respectively. The skin factors are 7.5662, 7.099 and 4.7738, respectively. The initial pressures are 6.01 Mpa, 6.02 Mpa and 5.58 Mpa, respectively. However, heterogeneity cannot be identified in either the Horner curve or the log–log di-

agnostic plot (Figure 7e), as there is no approximate horizontal line when the reservoir is highly heterogeneous.

3.5. Integrated Model

The simulated results from the integrated model are shown in Figure 8. From Figure 8a, it can be seen that the simulated data fit the field data well at the whole falloff. However, the maximum pressure (10.33 MPa) is smaller than the measured maximum pressure (10.928 MPa). The Pearson correlation coefficient is 0.94901. The gray coefficient degree is 0.831. This confirms that the CBM reservoir of well V01 in Hedong coalfield is a heterogeneous and stress-independent multilayer coal seam. Figure 8b shows the characteristics of the heterogeneous, multi-layered, and stress-independent model in mean time. Nevertheless, it is not identical to these models. Comparing to the other models, the maximum pressure at the end of falloff is most close to the field data (6.312 MPa). It is bigger than that in other models. However, it is smaller than that in the multilayer model. The maximum velocity at the end of falloff is lower than that in the heterogeneous and multilayer model while it is higher than that in stress-independent and homogeneous model. The investigation radius can be read from pressure distribution, which is 9.014 m.

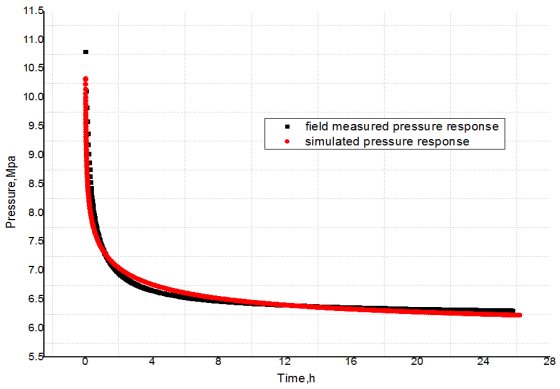

(**a**) Pressure–time curves

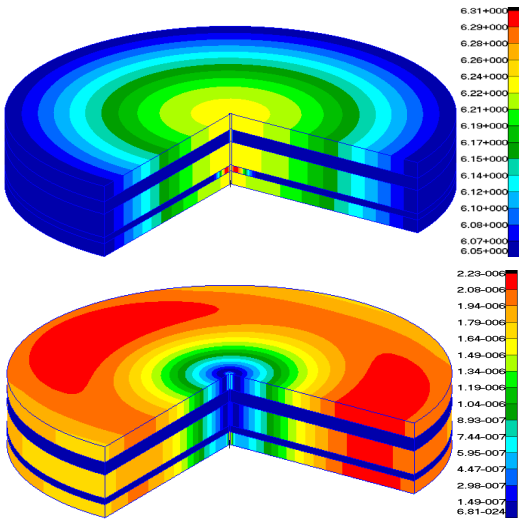

(**b**) Pressure and velocity distribution at the end of falloff

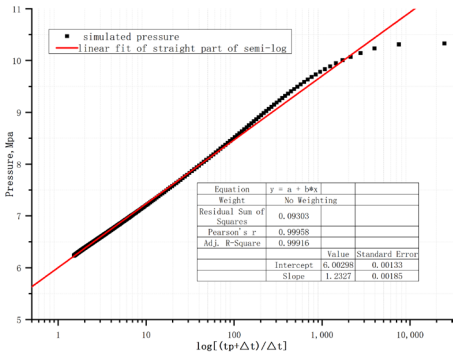

(**c**) Horner curve

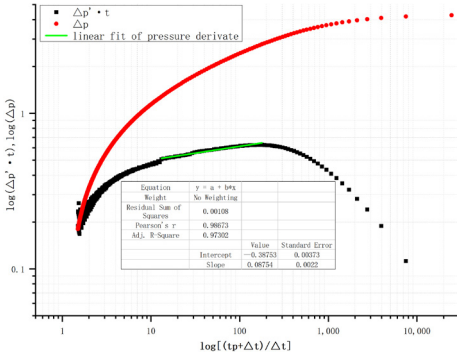

(**d**) Log–log diagnostic plot

Figure 8. Simulated results in integrated model.

From Figure 8c, the permeability of the integrated model can be obtained, which is 0.0693 md, 0.0041 md (5.6%) smaller than that we obtained from the field data. The initial pressure is 6.003 Mpa, which is 0.047 Mpa (0.78%) smaller than that we put into the model. Referring to Figure 8c,d, the skin factor is 7.424. An approximate horizontal line of slope 0.08754 with a radial fluid flow around the wellbore can be identified.

4. Discussion

The biggest difference between the log–log diagnostic/Horner curve analysis and the numerical-well-testing interpretation is permeability. It can reach up to 47.2% (in the heterogeneous model). As has been discussed in a previous publication [3,4], log–log diagnostic analysis is based on lots of assumptions which are far from the real reservoir. It also mainly focuses on the interpretation of mid- to late-period pressure data. In particular, it shows arbitrariness at the selection of the straight-line. Whether in theory or in field operation, the deficiencies are obvious. In all models, the simulated pressure–time curve stacks the field curve more or less in the mid- and late-period falloff. However, only in the integrated model is the highest approximation degree between the simulated data and field data achieved. This indicates that the field data are the multi-factor aggressive results. The more factors that are considered, the more reliable reservoir parameters can be obtained in the IFOT interpretation.

Numerical-well-testing interpretation addresses problems far beyond the reach of the log–log diagnostic analysis [4,5,7,22–26]. However, successful numerical-well-testing interpretation is greatly reliant on how close the model we built matches the real CBM reservoir. At same time, it also depends on the parameters we input into the model [4,5,10,22–26]. It is also the crucial factor for obtaining the simulated pressure response that has the best approximation degree to the field-measured results. However, most parameters input into the model come from field testing. Despite this, the effective thickness and viscosity of the testing fluid are difficult to select whether in the log–log/Horner analysis or numerical well testing.

To investigate the effective thickness, seven numerical experiments were conducted, in which the coal thickness were 2.5 m, 1.88 m, 1.75 m, 1.37 m, 1.13 m, 0.75 m, and 0.62 m, respectively. The simulated pressure –time curves are shown in Figure 9. It can be seen that the pressures at the late falloff match closely to the field data and each other, while at the middle falloff they are separated. The simulated pressure response of the 1370 mm thickness model matches with the field data best. Hence, 1370 mm can be thought of as the effective thickness in the tested well V01.

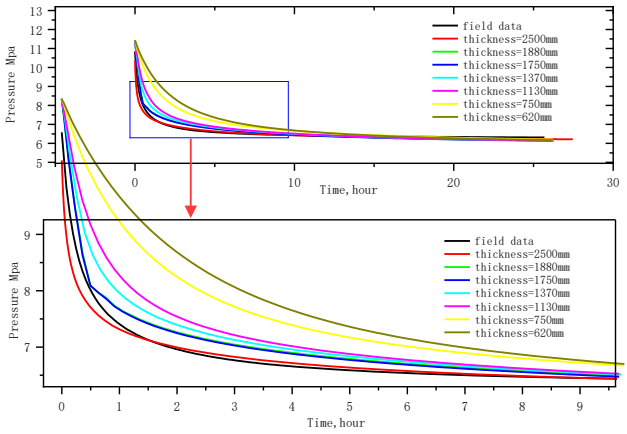

Figure 9. Pressure–time curves of different thickness.

Different falloff pressure curves with different viscosities were obtained, which are shown in Figure 10. As can be seen from Figure 10, at the early and late falloff, the simulated data with different viscosity are close to each other and near to the field data. However, they are different at middle falloff where the pressure increases with increasing viscosity. Considering that the Pearson correlation coefficient was maximum and the gray correlation degree was second largest when the viscosity was 0.5 mpa·s, the simulated pressure response with the viscosity of 0.5 mpa·s fit the field data best.

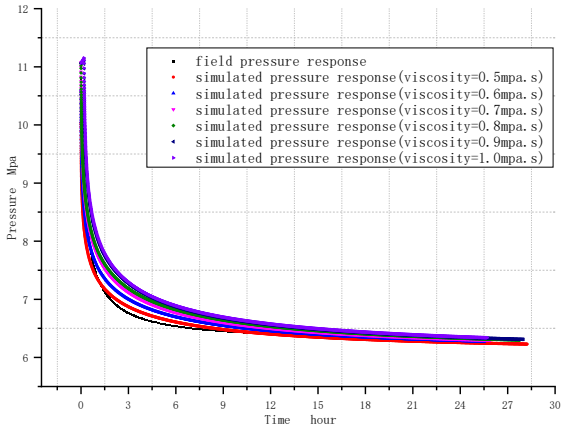

Figure 10. Pressure–time curves of different viscosity.

During the IFOT, the flow fluids in the CBM reservoir are made up of two parts. The first one is 2% kcl water or pure water injected from the ground. The second is the water in the coal seam. It is difficult to measure the viscosity of this mixture water; however, it can be approximated from the diagram which describes the relationship between viscosity and temperature [29]. According to the field-testing data, the temperature of the reservoir is 21.54 °C. Hence, the viscosity of coalbed water can be speculated as 0.78 mpa·s. Considering that some dissolved CBM might lower the viscosity, the viscosity of 0.5 mpa·s may be the reasonable viscosity of the tested fluid in the tested well.

5. Conclusions

Based on the field tested data of a CBM well in Hedong coalfield, seven groups of numerical experiments were performed. Our conclusions are summarized as follows:

(1) Evaluating the approximation degree between simulated pressure response and field data can be accomplished by using the Pearson correlation coefficient and gray correlation degree together.

(2) It is better to build an aggregative model in the numerical-well-testing interpretation of the CBM well. Otherwise, it is easy to drop into the pitfall of multi-results. After all, in all single-factor models, the simulated data are near to each other and close to the field data at early and late falloff.

(3) The effective thickness and viscosity of the testing fluid are also the crucial factors for obtaining the simulated pressure response with a high approximation degree to the field data.

(4) In the tested well V01, reservoir parameters with a higher reliability were obtained in the integrated numerical model, and the Pearson correlation coefficient and gray correlation degree between the simulated response pressure and field-measured data reached up to 0.94901 and 0.831. The permeability, initial pressure, skin factor and investigation radius were determined as 0.0424 md, 6.05 MPa, 7.424 and 9.014 m, respectively.

(5) Even in the integrated model, some discrepancies existed between the simulated data and field data. This indicates that some other factors were not taken into consideration, such as natural fracture, the temperature difference between the injected water and reservoir, a hydraulic fracture created during injection, and so on. In the future, the consideration on these factors in numerical-well-testing interpretation would be beneficial to obtain the CBM reservoir parameters with the highest reliability.

Author Contributions: X.Z. and S.F. conceived and designed the theory; X.Z., S.F. and Y.C. performed the experiment; Y.B. and S.F. analyzed the theory and data; X.Z. wrote the manuscript; D.M. reviewed the manuscript and searched conventional studies; B.H., X.L. and S.F. participated in the development

of the research plan and revised the manuscript. All authors have read and agreed to the published version of the manuscript.

Funding: The research was sponsored by National Natural Science Foundation of China (41902175).

Data Availability Statement: Not applicable.

Acknowledgments: The authors would like to express their gratitude to the editor and the reviewers for their helpful comments on the manuscript.

Conflicts of Interest: The authors declare no conflict of interest.

References

1. Zuber, M.D.; Sparks, D.P.; Lee, W.J. Design and Interpretation of Injection/Falloff Tests for Coalbed Methane Wells. In Proceedings of the Spe Technical Conference & Exhibition, New Orleans, LA, USA, 23–26 September 1990; pp. 425–434.
2. Hopkins, C.W.; Frantz, J.H.; Flumerfelt, R.W.; Spivey, J.P. Pitfalls of Injection/Falloff Testing in Coalbed Methane Reservoirs. In Proceedings of the SPE Permian Basin Oil and Gas Recovery Conference, Midland, TX, USA, 25–27 March 1998; pp. 9–24.
3. Seidle, P. *Fundamentals of Coalbed Methane Reservoir Engineering*; Penn Well Corporation: Tulsa, OK, USA, 2011.
4. Yao, J.; Wu, M.L. Numerical Well Testing Interpretation Theory and Method. In *Streamline Numerical Well Test Interpretation*; Elsevier: Amsterdam, The Netherlands, 2011; pp. 1–16.
5. Mahyapour, R.; Zargar, G.; Hashemi, A. Advances in well testing analysis using numerical well testing and reservoir simulation; a field case. *Sci. Int.* **2014**, *25*, 1461–1464.
6. McLean, K.; Zarrouk, S.J. Pressure transient analysis of geothermal wells: A framework for numerical modelling. *Renew. Energy* **2017**, *101*, 737–746. [CrossRef]
7. Amina, B. *Injection/Falloff Testing of Vertical and Horizontal Wells*; The Graduate School, The University of Tulsa: Tulsa, OK, USA, 2007.
8. Feng, Q.; Liu, J.; Huang, Z.; Tian, M. Study on the optimization of fracturing parameters and interpretation of CBM fractured wells. *J. Nat. Gas Geosci.* **2018**, *3*, 109–117. [CrossRef]
9. Liu, Y.W.; Ou-Yang, W.P.; Zhao, P.H.; Lu, Q.; Fang, H.J. Numerical well test for well with finite conductivity vertical fracture in coalbed. *Appl. Math. Mech.-Engl. Ed.* **2014**, *35*, 729–740. [CrossRef]
10. Pei, Y.L.; Kamy, S. Investigation of Parent-Well Production Induced Stress Interference in Multilayer Unconventional Reservoirs. *Rock Mech. Rock Eng.* **2022**, *55*, 2965–2986. [CrossRef]
11. Guo, X.; Wu, K.; Killough, J. Investigation of Production-Induced Stress Changes for Infill-Well Stimulation in Eagle Ford Shale. *SPE J.* **2018**, *23*, 1372–1388. [CrossRef]
12. Martirosyan, A.V.; Ilyushin, Y.V. Modeling of the Natural Objects' Temperature Field Distribution Using a Supercomputer. *Informatics* **2022**, *9*, 62. [CrossRef]
13. Bosikov, I.I.; Klyuev, R.V.; Mayer, A.V.; Stas, G.V. Development of a method for analyzing and evaluating the optimal state of aerogasodynamic processes in coal mines. *Sustain. Dev. Mt. Territ.* **2022**, *14*, 97–106. [CrossRef]
14. Bosikov, I.I.; Martyushev, N.V.; Klyuev, R.V.; Savchenko, I.A.; Kukartsev, V.V.; Kukartsev, V.A.; Tynchenko, Y.A. Modeling and Complex Analysis of the Topology Parameters of Ventilation Networks When Ensuring Fire Safety While Developing Coal and Gas Deposits. *Fire* **2023**, *6*, 95. [CrossRef]
15. Gou, B.; Wang, C.; Yu, T.; Wang, K. Fuzzy logic and grey clustering analysis hybrid intelligence model applied to candidate-well selection for hydraulic fracturing in hydrocarbon reservoir. *Arab. J. Geosci.* **2020**, *13*, 975–986. [CrossRef]
16. Chen, H.; Tian, W.; Chen, Z.; Zhang, Q.; Tao, S. Genesis of Coalbed Methane and Its Storage and Seepage Space in Baode Block, Eastern Ordos Basin. *Energies* **2022**, *15*, 81. [CrossRef]
17. Fang, S.Y.; Chen, Y.; Bao, Y.; Yang, X.; Ma, D. A new reliability evaluation method of injection/falloff testing interpretation in coal reservoir based on FAHP and cloud model. *Energy Sources Part A-Recovery Util. Environ. Eff.* **2020**. [CrossRef]
18. Tian, L.; Cao, Y.X.; Chai, X.; Liu, T.; Feng, P.; Feng, H.; Zhou, D.; Shi, B.; Oestreich, R.; Rodvelt, G. Best practices for the determination of low-pressure/permeability coalbed methane reservoirs, Yuwu Coal Mine, Luan mining area, China. *Fuel* **2015**, *160*, 100–107. [CrossRef]
19. *GB/T 24504-2009*; The Method of Injection/Falloff Well Testing for Coalbed Methane Well. Standardization Administration of the People's Republic China, National Standard of the People's Republic of China: Beijing, China, 2009. (In Chinese)
20. Lin, Y.; Qin, Y.; Ma, D.; Wang, S.; Qiao, J. In situ stress variation and coal reservoir permeability response of the Jurassic Yan'an formation in the southwestern Ordos basin, China: Its impact on coalbed methane development. *Geoenergy Sci. Eng.* **2023**, *222*, 211444. [CrossRef]
21. Liu, H.H.; Sang, S.X.; Sang, S.; Xue, J.; Wang, G.; Xu, H.; Ren, B.; Liu, C.; Liu, S. Characteristics of an in situ stress field and its control on coal fractures and coal permeability in the Gucheng block, southern Qinshui Basin, China. *J. Nat. Gas Sci. Eng.* **2016**, *36*, 1130–1139. [CrossRef]
22. Fan, Y.P.; Shu, L.Y.; Huo, Z.; Hao, J.; Yang, L. Numerical Simulation Research on Hydraulic Fracturing Promoting Coalbed Methane Extraction. *Shock. Vib.* **2021**, *2021*, 3269592.

23. Li, W.; Liu, J.S.; Zeng, J.; Leong, Y.K.; Elsworth, D.; Tian, J. A fully coupled multidomain and multiphysics model considering stimulation patterns and thermal effects for evaluation of coalbed methane (CBM) extraction. *J. Pet. Sci. Eng.* **2022**, *214*, 110506. [CrossRef]
24. Li, Q.; Xing, H.L. A new method for determining the equivalent permeability of a cleat dominated coal sample. *J. Nat. Gas Sci. Eng.* **2016**, *34*, 280–290. [CrossRef]
25. Palmer, I.; Mansoori, J. How Permeability Depends on Stress and Pore Pressure in Coalbeds: A New Model. *SPE Reserv. Eval. Eng.* **1998**, *1*, 539–543. [CrossRef]
26. Wang, X.K.; Sheng, J.J. Effect of low-velocity non-Darcy flow on well production performance in shale and tight oil reservoirs. *Fuel* **2017**, *190*, 41–46. [CrossRef]
27. Li, S.W.; Guo, M.Z.; Wang, L.; Chai, M.; Chen, F.; Wei, Y. Analysis on the Correlation Degree between the Driver's Reaction Ability and Physiological Parameters. *Math. Probl. Eng.* **2017**, *2017*, 5215874.
28. Sun, G.D.; Guan, X.; Yi, X.; Zhou, Z. Grey relational analysis between hesitant fuzzy sets with applications to pattern recognition. *Expert Syst. Appl.* **2018**, *92*, 521–532. [CrossRef]
29. Wang, C.Y.; Xiang, Y.; Deng, L.Z.; Shan, Y.M. *Petrophysics*; Sichuan Science & Technology Press: Chengdu, China, 2006.